THE ASTROPHYSICAL JOURNAL, 452:1–15, 1995 October 10

BIAS PROPERTIES OF EXTRAGALACTIC DISTANCE INDICATORS. IV. DEMONSTRATION OF THE POPULATION INCOMPLETENESS BIAS INHERENT IN THE TULLY-FISHER METHOD APPLIED TO CLUSTERS

ALLAN SANDAGE
The Observatories of the Carnegie Institution of Washington, 813 Santa Barbara Street, Pasadena, CA 91101
AND
G. A. TAMMANN AND MARTIN FEDERSPIEL
Astronomisches Institut der Universitat Basel, Venusstrasse 7, CH-4102, Binningen, Switzerland
Received 1995 January 4; accepted 1995 April 21

ABSTRACT

A demonstration is made of the existence of the Teerikorpi Cluster Population Incompleteness Bias (CPIB) in the Tully-Fisher (TF) method of distance determination. A bias exists if the cluster is sampled incompletely into its luminosity function, despite the fact that all the cluster galaxies are at nearly the same distance. Neglect of the bias will give too small a cluster distance and, therefore, too high a Hubble constant.

The bias is modeled using graphical methods based on properties of Spaenhauer diagrams following the method of Papers II and III. It is shown that the bias is the same as the individual $M_0 - M(m, z)$ corrections derived in Paper I, generalized to the $M_0 - M(m, v_{rot}, z)$ corrections in Papers II and III for the TF method.

Four predictions of the model are that (1) the slope of the *apparent* TF regression depends on how far we sample into the cluster luminosity function, (2) the highest rotators will lie closest to the unbiased fiducial TF ridge line, (3) the error in the distance modulus decreases as the magnitude grasp into the cluster luminosity function (LF) increases, reaching zero only at ~ 6 mag into the cluster LF if the intrinsic dispersion is as high as we obtain here, and (4) the *observed*, not the true, dispersion is a strong function of the sampling depth into the luminosity function. The small TF dispersions in clusters derived in a number of current discussions are artifacts of the bias caused by using incomplete samples.

The predictions are verified using two independent data samples of real galaxies.

Values of the Hubble constant near $H_0 = 90$ km s^{-1} Mpc^{-1} found using incomplete cluster data reduce to unbiased values between 45 and 55 when corrections for the cluster incompleteness bias are applied.

Subject headings: distance scale — galaxies: distances and redshifts — methods: statistical

> "*We do not know if this pedestrian argument suffices to change any minds, or whether it misses a point that is too subtle for us to have grasped thus far.*"
> Kurt Gottfried in a reply to a criticism by John Bell concerning the role of measurement in quantum mechanics (Physics World, 4, 34 [1991]).

1. INTRODUCTION

The purpose of this paper is to study the bias properties of incomplete, flux-limited samples of galaxies in clusters when such samples are used to derive cluster distances by the Tully-Fisher (TF) method. It was early believed that such samples suffer no bias errors in the resulting distances, even if the samples are incomplete because all galaxies in a given cluster are nearly at the same distance. This is the premise upon which many of the TF cluster distance scales are based (Aaronson et al. 1986; Aaronson & Mould 1986: Pierce & Tully 1988, 1992).

Nevertheless, that a bias does in fact exist was discussed theoretically by Teerikorpi (1987, 1990). Further, it was identified empirically by Kraan-Korteweg, Cameron, & Tammann (1988, hereafter KKCT) and Fouqué et al. (1990, hereafter FGBP) using Virgo Cluster data. Following Teerikorpi, we hereafter call the effect the "cluster population incompleteness bias" (abbreviated in what follows as the CPI bias or sometimes as the CPIB).

Both Kraan-Korteweg et al. and Fouqué et al. demonstrated that the derived distance modulus of the Virgo Cluster using the TF method changed from $m - M = 30.7$ to 31.7 as the apparent magnitude grasp of the sample was increased from $B_T = 11$ to 16 (KKCT, Fig. 6). We show in this paper that this effect *is* the CPIB.

It was then argued by Pierce & Tully (1992, their Fig. 6) and by Pierce (in Jacoby et al. 1992, their Fig. 12) that the effect does not exist. They contended that the systematic shift of the TF ridge lines faintward as the magnitude grasp into the Virgo Cluster data deepens (Fig. 4 of KKCT) is a result of adding background galaxies to the sample rather than due to CPI bias. The purpose of this paper is to show that the CPIB effect is real by demonstrating its presence in non–Virgo Cluster data where "background effects due to cluster infall" do not exist.

A confusion exists in the literature concerning the incompleteness bias. Sample statements denying its existence include "—because the galaxy samples are chosen from a cluster population which is generally all at the same distance, Malmquist bias does not occur" (Aaronson et al. 1980), or "work with clusters avoids the thorny issue of how to properly treat the Malmquist effect, because the galaxies in a cluster are generally at all the same distance ... it is likely that any sort of magnitude bias effects can be dispensed with entirely" (Aaronson et al. 1982), or "several ... possible sample biases, including the Malmquist effect, are considered and dismissed" (Aaronson et

al. 1986), or "with clusters we confine ourselves to a sample which is basically volume rather than magnitude limited, allowing us to circumvent the [bias] problem" (Aaronson et al. 1986).

These statements are incorrect. First, the bias is not the Malmquist effect. It is more complicated, depending on catalog magnitude limit, redshift, and line width when using the TF method (Sandage 1994a, b, hereafter Papers I and II; Federspiel, Sandage, & Tammann 1994, hereafter Paper III). Second, the statements confuse the properties of a sample that is distance limited with one in which all objects are at the same distance if that sample is incomplete. A purpose of this paper to demonstrate that the derived distance in the latter case depends on how much of the cluster luminosity function is sampled. This is known as the Teerikorpi CPI bias, but we develop its properties here in a different way than was done by Teerikorpi (1990).

The plan of the paper is to give a semitheoretical demonstration in § 2 based on Spaenhauer diagrams, generalized from the method set out in the papers I–III. The method is applied in §§ 3 and 4 to data from two different environments. One is a simulated cluster environment where questions of "background contamination," raised by Pierce (1992), do not exist, and the other is the Virgo Cluster. The conclusions are made using a comparison of the predictions with the systematics in the data themselves.

Encouraged by the close agreement of the predictions made in § 2 with the actual data used in § 3 from the large field galaxy sample of Mathewson, Ford, & Buchhorn (1992, hereafter MFB) we analyze again the data for the Virgo Cluster in § 4, showing the predicted change of the TF slope and the absolute magnitude of the zero point and of the apparent dispersion of the TF diagrams as the magnitude grasp into the cluster is pushed faintward. The tests show the same effects discovered by KKCT, by FBGP in Virgo, and explained by Teerikorpi (1990) with his theoretical model.

2. PREDICTIONS CONCERNING THE CLUSTER INCOMPLETENESS BIAS USING SPAENHAUER DIAGRAMS

2.1. *The Method*

The CPI bias is demonstrated here via Spaenhauer diagrams (SDs), one for each line width (LW) interval, following the methods in Papers II and III. ("Line width" and "rotational velocity" are related by LW $\sim 2\, v_{\rm rot}$). The method differs from the formalism of Teerikorpi (1987, 1990), Lynden-Bell et al. (1988), and Willick (1994), although we suspect the solutions are the same.

Proof of the existence of bias is made by adding progressively fainter data to the Spaenhauer diagrams and testing if the apparent bias properties move faintward as the apparent magnitude grasp of the sample increases. If bias exists, corrections for it can be made as functions of redshift, line width, and the apparent magnitude cutoff of the samples. These are the triple-valued (m, LW, redshift) corrections calculated in Papers II and III.

2.2. *Demonstration Using Simulated Clusters from the MFB Field Galaxy Sample*

The general problem solved in Papers II and III was to identify bias in samples of field galaxies that have a large range in distances.

The bias problem in the present paper is different because all cluster galaxies are at nearly the same distance. However, we show below that this is simply a special case of the general problem solved in Paper I, again leading to a bias if the intrinsic dispersion of the distance indicator is as large as we claim. The illustration of the problem and its solution is set up by considering that subset of a sample of *field* galaxies that have nearly the same redshift, imitating the condition of galaxies in a cluster.

Recall from Paper I (Fig. 4) that the calculation of the bias correction, $M_0 - M(m, v_i)$, at a given redshift v_i can be made from the Spaenhauer diagrams by considering the percentage of the luminosity function that is cut away by the apparent-magnitude limit line for the subsample contained in the redshift interval $dv_i/2$ at v_i. Recall also that the *gross* Malmquist bias is the sum over all velocity space of the individual $M_0 - M(m, v_i)$ corrections, weighted by the volume elements, $v_i^2\, dv_i$. However, as in Papers I–III, this integrated Malmquist factor is not the correction we need. Rather, we need *each* of the components of the integrand. These are the *individual* magnitude corrections at a particular redshift as the apparent magnitude limit for data in a given cluster is made progressively fainter.

We now demonstrate this claim and derive the properties of the CPI bias using the large TF sample by Mathewson et al. (1992). The method is to make several artificial clusters from the data as they are binned into separate narrow intervals of redshift, one for each artificial cluster defined by galaxies in the restricted redshift interval.

The bias properties of TF samples can be made manifest by considering individual Spaenhauer diagrams for narrow ranges of line width, one for each line width interval. This is the method of Paper III, to which the reader is referred for the details that are important here. We have adapted Figure 5 of that paper, adding several features useful for our present problem. We show it as Figure 1 here. Five ranges of line width are shown for the rotational velocity intervals of greater than 250 km s^{-1}, between 250 and 200 km s^{-1}, 150–200 km s^{-1}, 100–150 km s^{-1}, and less than 100 km s^{-1}.

The shapes of the individual Spaenhauer configurations have been copied from Paper I (Fig. 3), calculated with the indicated dispersions, $\sigma(M)$, determined from the "total" MFB data as used in Paper III. The ordinate is the kinematic absolute I magnitude calculated using $H_0 = 50$ (however, the absolute distance scale is irrelevant). The abscissa is the redshift referred to the centroid of the Local Group. An apparent magnitude limit of $I = 14$ is put in each diagram calculated from $m - M = 5 \log v + 16.5$, where the constant obtains if $H_0 = 50$ km s^{-1} Mpc^{-1}.

For an apparent magnitude limit this faint, no galaxies in the highest two line width bins (*upper and middle left panels*) are cut from the MFB sample, and the mean absolute data for them are unbiased. Note that this would not be the case if the apparent magnitude limit had been placed brighter at $I = 12.5$ as in Figure 6 of Paper III.

Bias to the *mean* absolute magnitude of the sample, i.e., summed over all redshifts, has begun at redshifts larger than $\log v = 3.6$ where the lower curved envelope line intersects the apparent magnitude limit line in the lower left panel of Figure 1. The bias is obvious in the two panels at the right which are for the lowest line widths.

Two vertical lines are drawn in Figure 1 showing a redshift interval in $\log v$ from 3.5 to 3.6. Galaxies in this interval are all

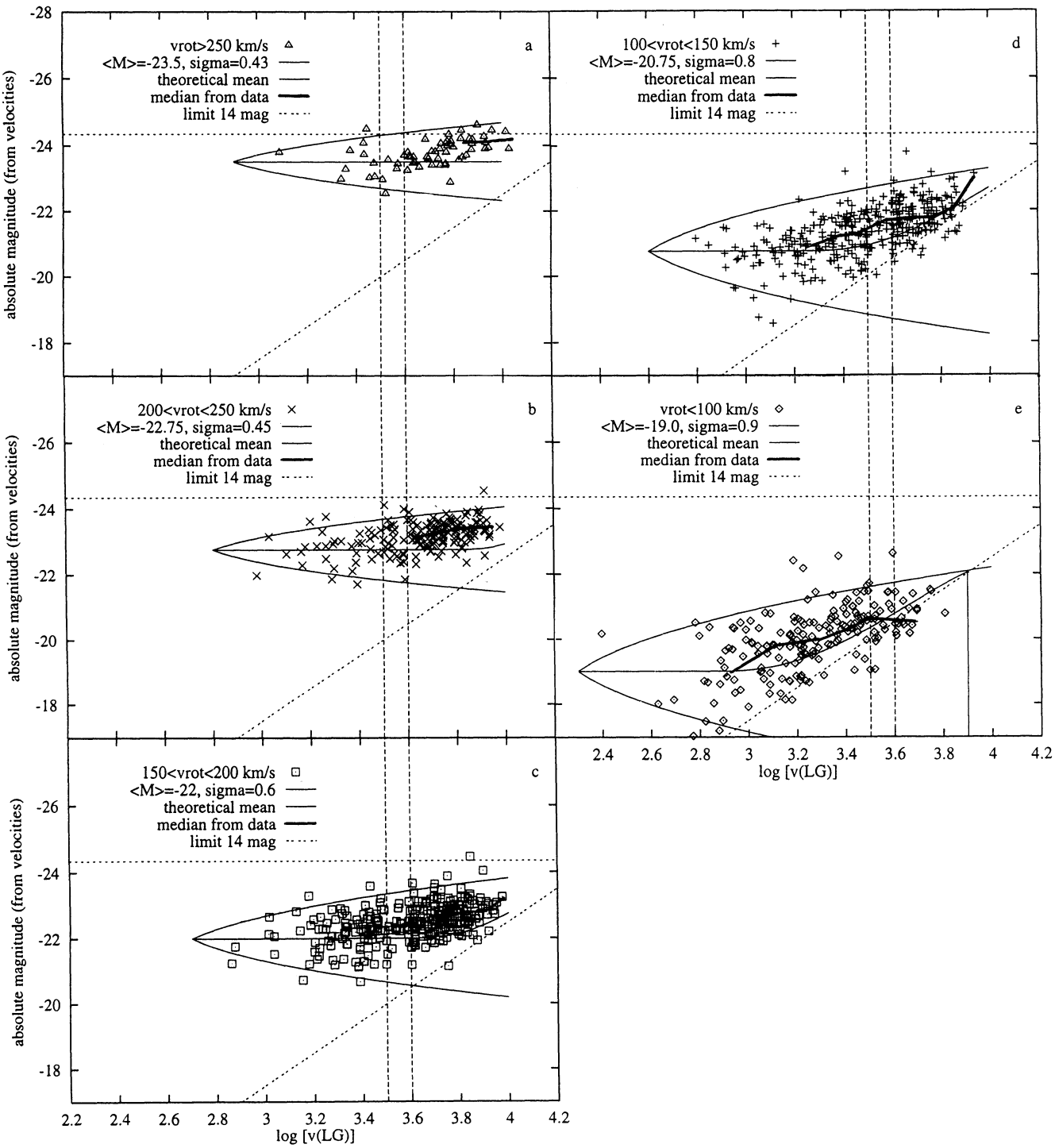

FIG. 1.—Fig. 5 of Federspiel, Sandage, & Tammann (1994 [Paper III], but with guiding lines as aids to understanding the model in the text. The two vertical lines cutting all panels show a simulated cluster, all "members" at a common distance. An apparent magnitude limit line of $I = 14$ is shown in each panel. The horizontal line tangent to the upper envelope of the configuration at log redshift = 3.55 in the upper left panel defines the absolute magnitude of the brightest galaxies in the simulated cluster. This line is repeated in each panel.

at approximately the same distance. The sample therefore imitates the conditions of a cluster. The dotted horizontal line placed at $M_I = -24.2$, repeated in each panel, is set tangent to the upper curved envelope in the upper left panel at the middle of the redshift interval defined by the two vertical lines. It is discussed later.

Various predictions of the expected correlations that illustrate the bias can be seen from Figure 1.

1. Galaxies with the largest rotational velocities, such as in the three Spaenhauer configurations in the left panels, are not biased *at the $I = 14$* faintness limit because each configuration

is sampled completely in the indicated redshift interval (log v between 3.5 and 3.6). However, galaxies in the two lower rotational velocity panels at the right are progressively biased because the $I = 14$ mag limit cuts into the configurations in the indicated narrow redshift interval.

The effect of this cut is that the slope of a linear TF relation for such "cluster" galaxies will be shallower than the true slope when the data are sampled only to $I = 14$ because part of the data at faint absolute magnitudes will be missing. Although the missing galaxies are also of low line width, nevertheless the absolute magnitudes of the galaxies remaining in the sample *at these line widths* will be brighter than the unbiased $\langle M_0 \rangle$ magnitude at that line width, shown by the lines through the middle of the configurations. This affects the slope, making it shallower, as said, than that of the true (unbiased) TF regression. This prediction on the slope effect is the same as is seen in Figures 4 and 7 of Paper II, read at any fixed redshift.

2. As the magnitude limit is made fainter, the *range* of rotational velocities within which the data will lie above the magnitude-limit line will become larger (cf. Figs. 5–6 of Paper III). Data in this range will be unbiased. The result is that the smaller LW data will become progressively more unbiased the fainter the apparent magnitude cut is. The highest rotational velocities will be closest to the unbiased ridge line in a TF diagram at a given limiting apparent magnitude, whereas the slower rotators will not. Hence, the *apparent* TF relation will appear to be nonlinear (if in fact the true relation is linear), curving toward the unbiased ridge line asymptotically at the highest LWs (Figs. 4 and 7 of Paper II).

3. The bias will cause a change in the *zero point* of the mean absolute magnitude of those galaxies that remain in each subset as the catalog apparent magnitude limit is made fainter. Only galaxies whose rotational velocities are high enough (as in the three left panels of Fig. 1) will be bias free. These are the only galaxies for which the correct mean absolute magnitude, M_0(LW), that must be used at each redshift and line width to obtain unbiased distances is the *apex* magnitude. For all other galaxies in the sample at redshifts larger than the distance-complete limit, the $M(m, v_{\rm rot}, z)$ absolute magnitudes must be used to obtain statistically correct distances that are not compressed by the bias.

To find how far into the luminosity function we must reach to be complete at each line width, draw a horizontal line tangent to the upper envelope at log $v = 3.55$ in the upper left Spaenhauer configuration of Figure 1. This defines the *brightest galaxy* in the simulated cluster. Repeat this horizontal line in each of the panels, keeping the absolute magnitude level the same. Read, then, the *magnitude difference* between this line and the *lower curved envelope-limit line* in each configuration to find the magnitude that must be sampled into the cluster if we are to avoid incompleteness bias.

From this construction, we see that the magnitude grasp into a cluster that is required to be bias free, using the dispersion of each SD shown in Figure 1, must be ~ 1.8 mag into the luminosity function for the upper left panel, ~ 4 mag for the lower left panel, ~ 5.5 for rotational velocities between 100 and 150 km s^{-1} in the upper right, and ~ 8 mag for the slowest rotators in the lower right panel.

4. The *apparent* dispersion of the TF correlation calculated from the *biased* sample will be smaller than that for a distance-limited sample for two reasons: (*a*) the intrinsic dispersion is smallest for the fastest rotators (the widths of the configurations in Fig. 1 are larger for the slower rotators), and (*b*) the apparent dispersion of the subset of the sample that remains above the limit line in each of the biased configurations becomes progressively smaller as the rotational velocity decreases, seen well in the lower right-hand panel of Figure 1.

To test these four predictions, of which the third and fourth lead incorrectly to the short distance scale if uncorrected, we now discuss the MFB field galaxy data, binned into discrete redshift intervals so as to simulate a series of clusters at different redshifts.

3. DEMONSTRATION OF THE BIAS USING SIMULATED CLUSTERS FROM THE MFB FIELD GALAXY SAMPLE

We now analyze the data of MFB by isolating several subsamples contained within several narrow redshift intervals. If bias effects are present they will move faintward by 1 mag for each increase of the redshift interval by 0.2 dex. This is equivalent to sampling several real clusters at different redshifts to different grasps into their luminosity functions, if the apparent magnitude catalog limits are kept constant.

The bias problems affect both (1) the proper mean absolute magnitude to use to obtain statistically correct mean photometric distances, and (2) the determination of the intrinsic dispersion of the TF relation from the observed (apparent) dispersion as functions of the percentage of the complete luminosity function that is sampled (or, equivalently, that is missing).

Consider first a subsample of the MFB data that exists in the redshift interval between log v_i of 3.4–3.6. The observer's procedure of adding fainter galaxies to a real cluster catalog is simulated by changing the catalog magnitude limit by adding progressively fainter galaxies from the MFB field sample, keeping the stated redshift interval fixed. We test the four predictions from § 2 as fainter galaxies are added from this sample.

Figure 2 shows the result using five Tully-Fisher diagrams for the simulated cluster in the redshift interval $3.4 < \log v < 3.6$. Figure 3 shows the same result for the simulated cluster in the redshift interval $3.6 < \log v < 3.8$. Calculations were also made for the nearer redshift interval of $3.2 < \log v < 3.4$. The results are used later (see Table 1) but are not shown as a diagram.

The progressive apparent magnitude limits in Figures 2 and 3 are $I < 11$ mag, < 12, < 12.5, < 13, and finally the total sample which contains galaxies (although incompletely) to the MFB limit at $I \sim 14.5$ mag.

The unbiased fiducial ridge line derived in Paper III (Fig. 7 and eq. [4b] there) is shown as the lower envelope line in each panel. Its equation is

$$M_I = -7.74 \log v_{\rm rot} - 4.69 \, . \qquad (1)$$

Verification of the four predictions made in § 2 are seen from Figures 2 and 3 as follows.

1. The slope of the least-squares regression that would be put through the *data themselves* is a function of the apparent magnitude cutoff adopted for the simulated cluster data. The equations of such regression lines for the direct TF relation (absolute magnitude as the independent variable) are listed in column (2) of Table 1. Data for the three simulated clusters with different redshifts are shown. Note that the slope values

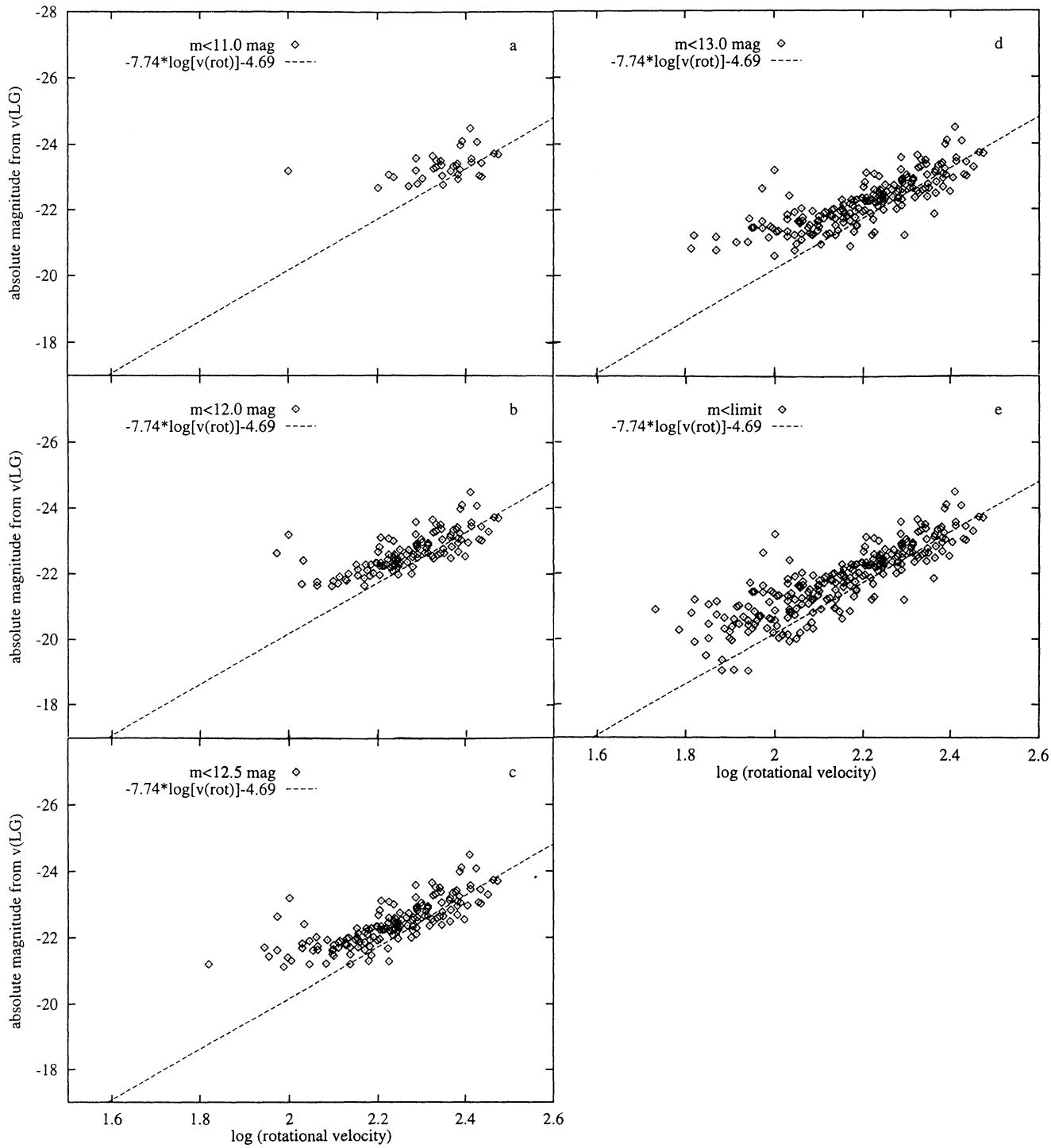

FIG. 2.—TF diagrams for the simulated cluster at a mean redshift of $\langle \log v \rangle = 3.5$ for five increasingly deeper grasps into the luminosity function. The actual MFB data in this redshift interval are used. The distance-limited unbiased TF direct regression of eq. (1) is drawn in each panel. The progressive deviation of the data from the unbiased line at each rotation velocity *is* the Teerikorpi CPI bias. These deviations are listed in Table 1.

for each cluster change progressively as the catalog limiting magnitudes become fainter. For example, the slopes for the $3.4 < \log v < 3.6$ simulated cluster (Fig. 2) change from $dM/d \log v = -1.97$ for data with $m_I < 11$ mag to $dM/d \log v = -5.58$ when all the data are used. These slopes approach the unbiased slope of -7.74 that is valid for a *distance-limited* sample (eq. [1]) as the magnitude grasp into the cluster increases. However, they do not reach it even when the total sample is used because part of that sample is still incomplete, suffering from "cluster incompleteness bias" even at the limit of the MFB data.

2. Galaxies with the highest rotational velocities lie closest to the unbiased line, and vice versa, seen directly by inspection of Figures 2 and 3.

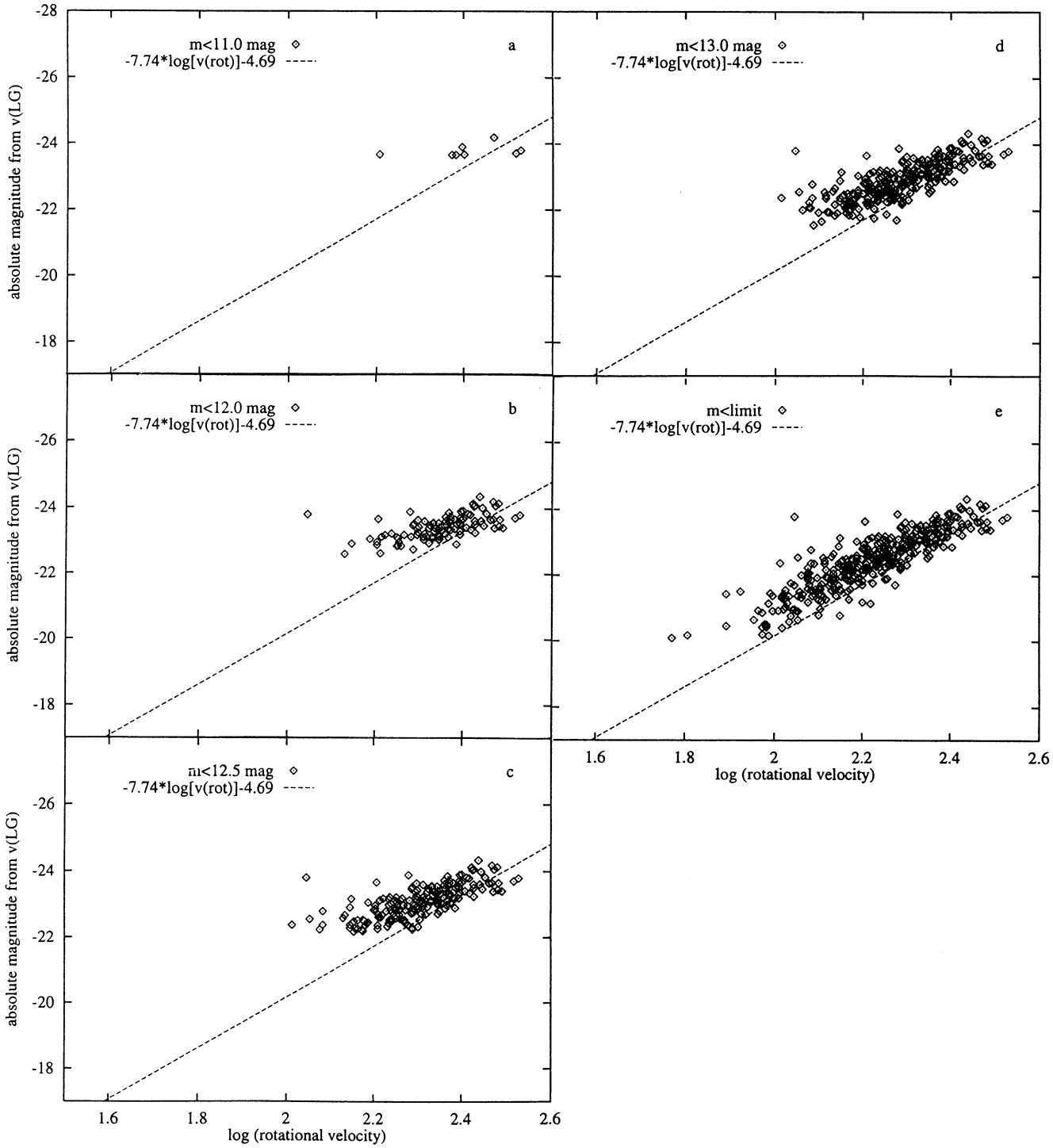

FIG. 3.—Same as Fig. 2, but for a simulated cluster at the larger distance at the mean redshift of ⟨log redshift⟩ = 3.7. Note that the deviations of the data from the unbiased line are larger than in Fig. 2. The reason is that, at a given cut in apparent magnitude, the depth of sampling into the luminosity function is less than in Fig. 3.

3. The magnitude difference between the unbiased line of equation (1) in Figures 2 and 3 and the mean line through the data in each panel, read at any particular v_{rot} value, is the bias correction, $M_0 - M(m, v_{rot}, \text{redshift})$, calculated in Papers II and III. Clearly, the $M_0 - M(m, v_{rot}, z)$ corrections depend on v_{rot}. Galaxies with higher rotational velocities are closer to the unbiased line than those with low v_{rot}. Therefore, these have the smallest bias corrections.

These magnitude differences (eq. [1] minus the equations in Table 1 at a given v_{rot}) are listed in columns(6)–(8) of Table 1 at the three values of the rotational velocity of log V_{rot} = 2.0, 2.2, and 2.4, for each of the three simulated clusters. The magnitude

TABLE 1

LINEAR LEAST-SQUARES TF REGRESSIONS FOR THREE SIMULATED MFB CLUSTERS

MAGNITUDE LIMIT (1)	SOLUTION (2)	N (3)	$\sigma(M_I)$ (4)	ΔM (5)	$\Delta(m-M)$ log v_{rot} = 2.0 (6)	$\Delta(m-M)$ log v_{rot} = 2.2 (7)	$\Delta(m-M)$ log v_{rot} = 2.4 (8)
Cluster $3.2 < \log v < 3.4$							
<11.0	$-2.48 \log V_{rot} - 16.87$	46	0.42	2.0	...	0.61	...
<12.0	$-4.09 \log V_{rot} - 13.02$	97	0.52	3.0	1.03	0.30	...
<12.5	$-4.73 \log V_{rot} - 11.49$	127	0.55	3.5	0.78	0.18	...
<13.0	$-5.00 \log V_{rot} - 10.85$	153	0.57	4.0	0.68	0.13	...
<limit	$-5.50 \log V_{rot} - 8.74$	185	0.58	5.5	0.57	0.12	...
Unbiased	$-7.74 \log V_{rot} - 4.69$	...	0.62	∞	0.00	0.00	0.0
Cluster $3.4 < \log v < 3.6$							
<11.0	$-1.97 \log V_{rot} - 18.71$	35	0.37	1.25	...	1.32	0.17
<12.0	$-4.16 \log V_{rot} - 13.23$	118	0.40	2.25	...	0.66	−0.06
<12.5	$-4.35 \log V_{rot} - 12.72$	161	0.42	2.75	1.25	0.57	−0.11
<13.0	$-4.56 \log V_{rot} - 12.16$	196	0.45	3.25	1.11	0.47	−0.17
<limit	$-5.58 \log V_{rot} - 9.80$	254	0.55	4.75	0.79	0.36	−0.08
Unbiased	$-7.74 \log V_{rot} - 4.69$	...	0.62	∞	0.00	0.00	0.00
Cluster $3.6 < \log v < 3.8$							
<11.0	$-0.66 \log V_{rot} - 22.18$	8	0.17	0.50	...	...	0.49
<12.0	$-2.43 \log V_{rot} - 17.69$	106	0.29	1.50	...	1.32	0.25
<12.5	$-3.64 \log V_{rot} - 14.71$	197	0.33	2.00	1.82	1.00	0.18
<13.0	$-4.39 \log V_{rot} - 12.89$	272	0.36	2.50	1.50	0.83	0.16
<limit	$-5.82 \log V_{rot} - 9.54$	378	0.42	3.00	1.01	0.62	0.24
Unbiased	$-7.74 \log V_{rot} - 4.69$	...	0.62	∞	0.00	0.00	0.00

grasp into the luminosity function of each of the clusters is listed in column (5), calculated in the manner described in § 2, based on the construction in Figure 1, done separately for each of the simulated clusters. The grasp into the luminosity function is, of course, smaller at a given apparent magnitude cutoff at the higher redshifts.

The data on the magnitude corrections, now expressed as the *errors in the distance modulus*, $\Delta(m - M)$, as a function of line width are combined in Figure 4 for the three clusters as a function of the magnitude sampled into the luminosity function, starting with its brightest member, again using the construction in Figure 1 to define the brightest member. The curves in Figure 4 are made from smoothed[1] values of the data from columns (6)–(8), of Table 1, together with calculations, not shown, for other values of log V_{rot} such as 2.3 and 2.1.

The *apparent* dispersion, $\sigma(M)_{obs}$, is a function of the apparent magnitude grasp into the cluster luminosity function. Table 1 shows that the dispersion that would be observed is smallest for the brightest limiting magnitude in all three simulated clusters. Its values for the nearby cluster ($3.2 < \log v < 3.4$) changes from 0.42 to 0.58 mag as the apparent magnitude limit changes from $I < 11.0$ to the limit near $I = 14.5$.

The observed dispersions are different clusters using the *same* apparent magnitude cut. The reason is that the same bias properties move faintward at the rate of 1 mag per 0.2 dex in redshift, consistent with the requirements of the bias model. Said differently, at a fixed apparent magnitude limit, the fraction of the total luminosity function that is sampled differs between the three simulated clusters. We probe deeper into the

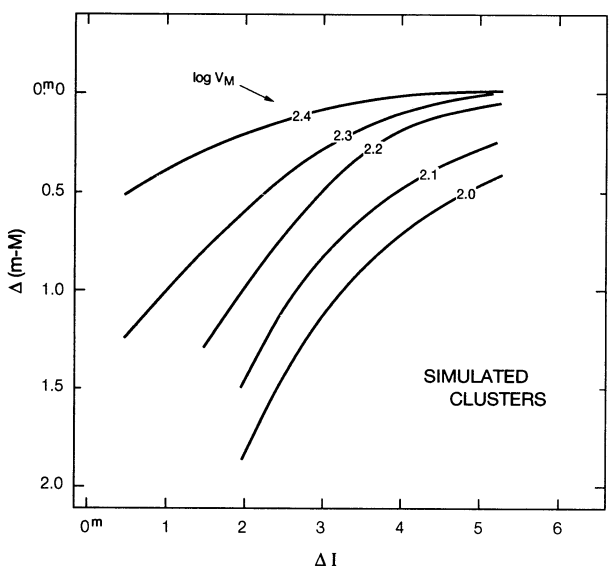

FIG. 4.—The error in the distance modulus as a function of the range of the luminosity function that is sampled in the three simulated clusters using the data in Table 1. The data in Table 1, per cluster, are shifted by 1 mag for each 0.2 dex increase in redshift to combine the data from the three clusters. The rotational velocities at the reading points of the equations in Table 1 are denoted as V_M.

[1] Cognizance has been taken in Fig. 4 of the fact that *linear* least-squares solutions should be replaced with nonlinear solutions at high V_{rot} values such that no negative values of $\Delta(m - M)$ are permitted. The actual curves in Figs. 2–3 must approach the unbiased line *asymptotically* at high V_{rot} values. Linear least-squares solutions near the high V_{rot} limit do not satisfy this requirement. They cross the unbiased line at negative $\Delta(m - M)$ values for high V_{rot}, which is an artifact of the linear solution. This defect of the linear solution has been compensated for in Fig. 4 for the highest line widths used.

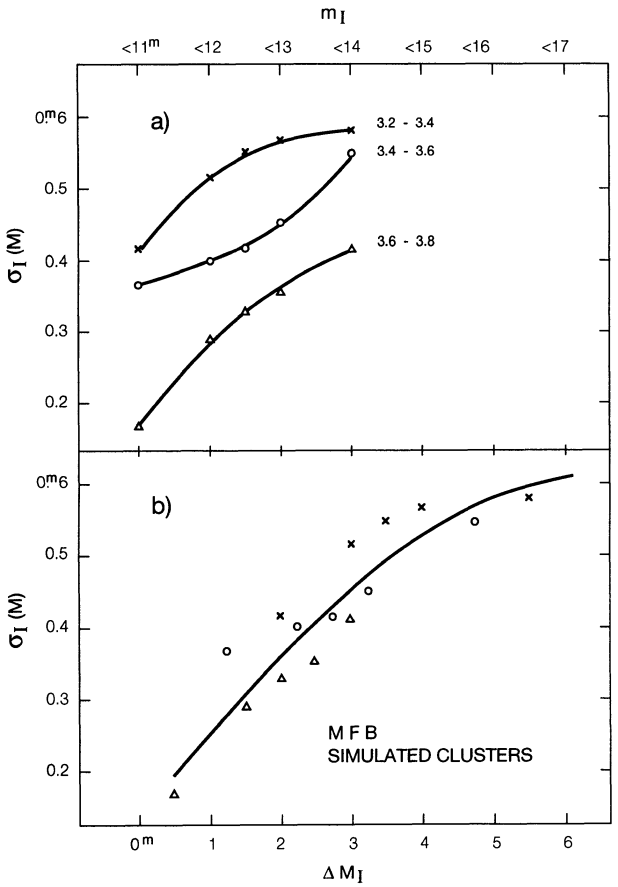

FIG. 5.—*Top*: Variation of the observed dispersion in M_I with apparent magnitude limit for the three simulated clusters. Data are from Table 1. *Bottom*: Combination of the three top curves by shifts of 1 and 2 mag accounting for the different redshifts of the clusters. The abscissa is the depth sampled into the luminosity function. The *true* dispersion, $\sigma(M)$, at a given line width is not seen in the observations until we sample ~6 mag into the luminosity function.

function for the nearby cluster than for the most distant if the apparent magnitude limit is kept constant.

Using the fact that the bias properties move brightward with increasing redshift for a *fixed* apparent magnitude limit, we can combine the results in columns (6)–(8) of Table 1 (these are the curves in Fig. 5*a*) to find the run of the dispersion as the absolute magnitude penetration into the luminosity function is increased.[2] (Note that the depth penetrated into the luminosity function is listed in col. [5] for each of the simulated clusters).

Figure 5 shows the result. The top panel shows the $\sigma(M)$ values for each of the three redshift intervals as a function of the apparent I magnitude (col. [1] of Table 1). The bottom panel shows the result of combining the data by shifting the curve for the 3.4–3.6 cluster to the right by 0.75 mag and for the 3.2–3.4 cluster by 1.50 mag. The shifts compensate for the different redshifts of the clusters at the rate of 1 mag per 0.2 dex in redshift, modified by the change in the absolute magnitude of the first ranked galaxy as a function of redshift (see footnote 2).

The abscissa of the bottom panel of Figure 5 is the magnitude difference that the presentation reaches from the brightest galaxy in the clusters, calculated by noting that the apparent magnitude of the intersection of the tangent line to the upper envelope of the SD at $\langle \log v \rangle = 3.55$ is at absolute magnitude ~ -24.2 from Figure 1. Using $m = M + 5 \log v + 16.5$, the corresponding apparent magnitude is $I = 10$. This is taken as the fiducial *zero point* (i.e., the point at which $\Delta M_I = 0$) in Figure 5*b*.

The importance of this diagram is that it counters the claims of Aaronson et al. (1980, 1982, 1986), Aaronson & Mould (1986), and Pierce & Tully (1988, 1992) that the *intrinsic* dispersion of their TF cluster data is only $\sigma(M) \sim 0.25$–0.4 mag.[3]

Figure 5*b* shows the disappointment of these claims. Most of the clusters used by Aaronson & Mould (1986) to derive their high value of H_0 were probed only 2–3 mag into the respective cluster luminosity functions (see § 5). Only 2 magnitudes are effectively broached in the data used by Pierce & Tully (1988, their Fig. 1) for the Virgo Cluster.

Figure 5*b* shows that the *observed* dispersion is only ~60% of the *intrinsic* value of the cluster grasp is only $\Delta I = 2$ mag. Six magnitudes must be sampled to reach the intrinsic dispersion.

4. DEMONSTRATION OF THE CPI BIAS IN THE TULLY-FISHER RELATION USING A FLUX-LIMITED SAMPLE OF VIRGO CLUSTER GALAXIES THAT IS COMPLETE

The conclusions concerning the Teerikorpi CPI bias in §§ 2 and 3 had previously been demonstrated by KKCT and FBGP using actual Virgo Cluster data.

Criticisms of the Virgo discussions have ranged from suggesting (1) that the KKCT magnitude data are inadequate for the demonstration (Burstein & Raychaudhury 1989), (2) that there is a severe depth effect (Pierce & Tully 1992) because of background and foreground infalling segments of the cluster, causing the observed large dispersion of the TF relation to be unreal, and (3) that the true dispersion about the ridge line of the TF relation is as small as $\sigma(M) = 0.3$ mag, making the bias problem for TF distances nearly moot (Pierce 1992; Bernstein et al. 1994).

The model in § 2 applied to the MFB simulated cluster data disappoints these criticisms.

1. The Virgo data used by KKCT do not suffer from the effects suggested by Burnstein & Raychaudhury, otherwise the bias properties predicted in §§ 2 and 3 based on an ideal cluster model would not be present. They are in fact present in the actual Virgo data in conformity with the ideal model. Furthermore, the same predicted effects seen by KKCT were found

[2] The ΔM values in col. (5) of Table 1 do not increase as 1 mag per 0.2 dex in log redshift for the following reason. The col. (5) values are the magnitude differences from the *brightest cluster member* at the listed apparent magnitude limits listed in col. (1). The brightest cluster member in the simulated clusters increases in luminosity as the redshift increases as a result of the increasing volume normalization factor. This brightening is given by the upper envelope of the Spaenhauer diagrams in Fig. 1 in each of the upper left panels read at $\langle \log v \rangle = 3.3$, 3.5, and 3.7. This brightening amounts to 0.25 mag for the 3.4–3.6 "cluster" and 0.5 mag for the 3.6–3.8 "cluster" relative to the 3.2–3.4 "cluster." In real clusters this is equivalent to the "cluster richness correction" (Sandage 1975).

[3] If the intrinsic dispersions were in fact this small, the bias problems would, of course, be nearly moot. The main difference between our current precept and that argued by Aaronson & Mould (1986) and Pierce & Tully (1988, 1992) for the short distance scale concerns this value of the *intrinsic*, not the observed, dispersion of the TF relation. They claim a small intrinsic dispersion. We say it is significantly large at a level of at least $< \sigma(M)_B > \sim 0.7$ mag.

later by FBGP, who used even better photometric data than those of KKCT for the Virgo Cluster. Again, the agreement of the data with the predictions concerning them belie the criticism by Burnstein & Raychaudhury.

2. There are no depth and/or putative infall or streaming effects *in the MFB simulated clusters.* The predictions based on the CPI bias model are the same as are *observed* in the Virgo data. Hence, Virgo data are not falsified by infall effects because no such effects are present in the analysis of §§ 2 and 3.

3. The large observed dispersions in the Virgo TF relation cannot be a result of adverse effects of any putative streaming or random motions on the absolute magnitudes used in Figures 1 and 2 for the reasons discussed in Paper I (footnote 1), Paper II (§ 2.2), and Paper III (§ 8.2). Any possible streaming and random motions give the *opposite sign* from that observed for the *scatter* in the Hubble diagram as a function of redshift. Hence, the criticisms concerning the large observed dispersion on the basis of streaming motions are not correct on the proffered grounds.

The demonstrations by KKCT and FBGP using their nearly complete data for the Virgo Cluster are decisive in showing that the CPI bias exists. In addition, the FBGP Virgo data can be used with the model in § 2 to (1) address how far into the luminosity function we must sample before the observed dispersion, $\sigma(M)$, is the *intrinsic* dispersion (similar to Fig. 6 of KKCT but using Virgo data as in Fig. 8 later), and (2) determine the size of the error in the distance modulus for different depths of sampling into the cluster luminosity function using the Virgo Cluster data themselves to obtain the equivalent of Figure 6. To do this we redetermine Figure 6 of KKCT using the FBGP data from their Table 2.

Figure 6 shows the equivalent of Figures 2 and 3 but using the *B* photometric band data for the Virgo Cluster. The absolute magnitudes are based on a distance modulus of $(m - M)_0 = 31.7$, but making the B_{T_c} listings of FBGP fainter by 0.19 mag to account for their assumed 0.19 mag absorption in *B* in the Galactic pole, which we set to zero.

The fiducial line drawn in each panel is the least-squares direct regression for the "complete" data in the lower right panel, reaching to apparent magnitude 16. This is 7.5 mag into the luminosity function. It is a more complete sample than was used by Pierce & Tully (1988, their Fig. 1) where their data encompassed only a range of ~2.5 mag into the luminosity distribution.

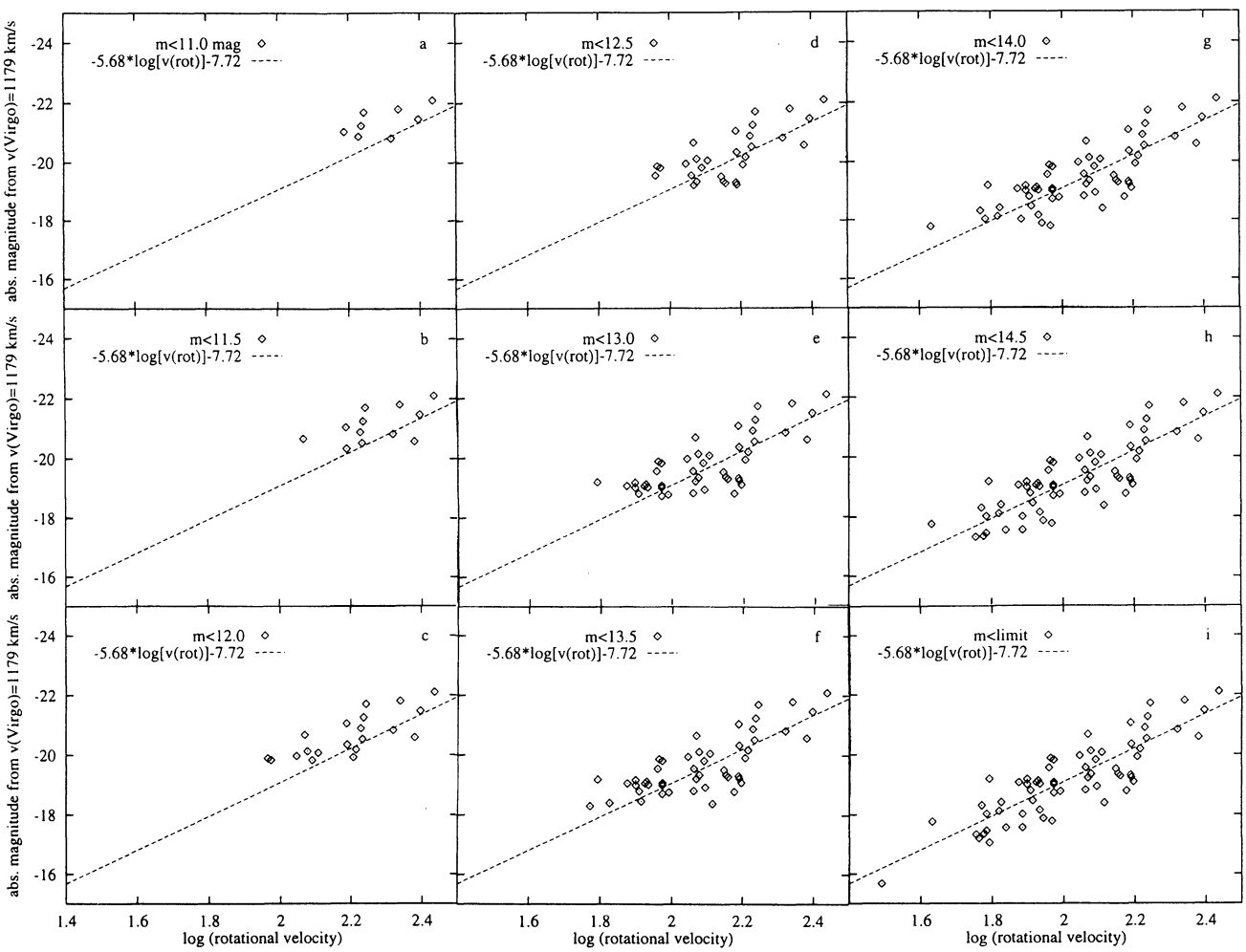

FIG. 6.—Same as Figs. 2 and 3, but for Virgo Cluster data in the *B* photometric band from FBGP. The line in each panel is the (direct) regression for the complete sample shown in the lower right panel, defining in first approximation the unbiased TF relation. Its equation is $M_B = -5.68 \log v_{rot} - 7.72$. Note that the definition of v_{rot} is that of FBGP, differing slightly from other definitions in the literature, requiring a conversion when using data based on a different LW system.

TABLE 2

LINEAR LEAST-SQUARES TF REGRESSIONS FOR THE VIRGO CLUSTER USING THE DATA OF FOUQUÉ ET AL.

					$\Delta(m-M)$		
MAGNITUDE LIMIT (1)	SOLUTION (2)	N (3)	$\sigma(M_B)$ (4)	ΔM (5)	log V_{rot} = 2.0 (6)	log V_{rot} = 2.2 (7)	log V_{rot} = 2.4 (8)
<11.0	$-2.05 \log V_{rot} - 16.81$	15	0.41	1.5	1.83	1.10	0.38
<11.5	$-3.26 \log V_{rot} - 13.85$	22	0.49	2.0	1.29	0.81	0.32
<12.0	$-4.11 \log V_{rot} - 11.77$	34	0.51	2.5	0.91	0.59	0.28
<12.5	$-4.32 \log V_{rot} - 11.11$	48	0.63	3.0	0.67	0.40	0.13
<13.0	$-4.48 \log V_{rot} - 10.60$	70	0.67	3.5	0.48	0.24	0.00
<13.5	$-4.67 \log V_{rot} - 10.10$	85	0.68	4.0	0.36	0.16	0.00
<14.0	$-4.61 \log V_{rot} - 10.15$	102	0.71	4.5	0.29	0.08	0.00
<14.5	$-4.92 \log V_{rot} - 9.41$	121	0.74	5.0	0.17	0.00	0.00
Limit	$-5.68 \log V_{rot} - 7.72$	131	0.78	7	0.00	0.00	0.00

The equation of the fiducial line in Figure 6 is

$$M_B = -5.68 \log v_{rot} - 7.72 , \quad (2)$$

as set out in the last listing in Table 2.

The data, cut at the indicated magnitude limits, are plotted in the nine panels of the diagram. The direct least-squares regressions are listed in Table 2, showing how the apparent dispersion, $\sigma(M)$, for each of the data subsets changes with the magnitude limit of the sample.

The mean magnitude offset from the fiducial line tabulated there is similar to those in Figure 2 and 3 for the simulated clusters. These offsets *are* the CPI biases. They decrease with increasing magnitude grasp into the cluster, approaching zero for the $\Delta(m - M)$ error in the modulus as the completeness of the sample increases.

The *magnitude differences* from the fiducial line of equation (2) are shown in Figure 7*a*. The family of curves is calculated from the equations in Table 2 as read at the indicated log V_{rot} values ranging from 1.9 to 2.4. Table 2 only lists these $\Delta(m - M)$ differences for log V_{rot} = 2.0, 2.2, and 2.4 in columns (6)–(8), but the complete family is shown in Figure 7*a*. The range from log V_{rot} = 1.9–2.4 is consistent with the range of the log V_{rot} values covered by the data. The distribution of the log V_{rot} values peak near log V_{rot} = 2.0; FBGP, Fig. 1.)

The apparent magnitude limits are marked along the top of Figure 7*a*. The depth sampled into the cluster, marked along the bottom, follows by adopting the brightest cluster galaxy to have B_{Tc} = 9.5 from Table 2 of FBGP.

Figure 7*b* shows the calculation of the "effective" magnitude offsets. These are the values of the mean modulus errors as a function of the depth sampled into the LF. The values are obtained by *averaging over all abscissa values* in each of the panels of Figure 6, calculated by finding the magnitude offset of *each* data point from the fiducial line and averaging the result. This is what an observer would calculate from a complete set of data obtained by adopting a particular slope to a fiducial TF relation as in Figure 6 and equation (2) and using that fiducial line to determine TF distances, biased as they would be by the CPIB effect.

Consider next the results for the Virgo Cluster concerning how the observed dispersion, $\sigma(M_B)$, approaches the intrinsic dispersion as the depth into the luminosity function is increased. The apparent dispersions displayed in Table 2 (col. [4]) for the data in the panels of Figure 6 are plotted in Figure 8. The FBGP B-band magnitudes (made fainter by 0.19 for zero absorption in the pole) are marked along the bottom. The depth penetrated into the luminosity function, based on the brightest cluster galaxy being at B = 9.5, is marked along the top.

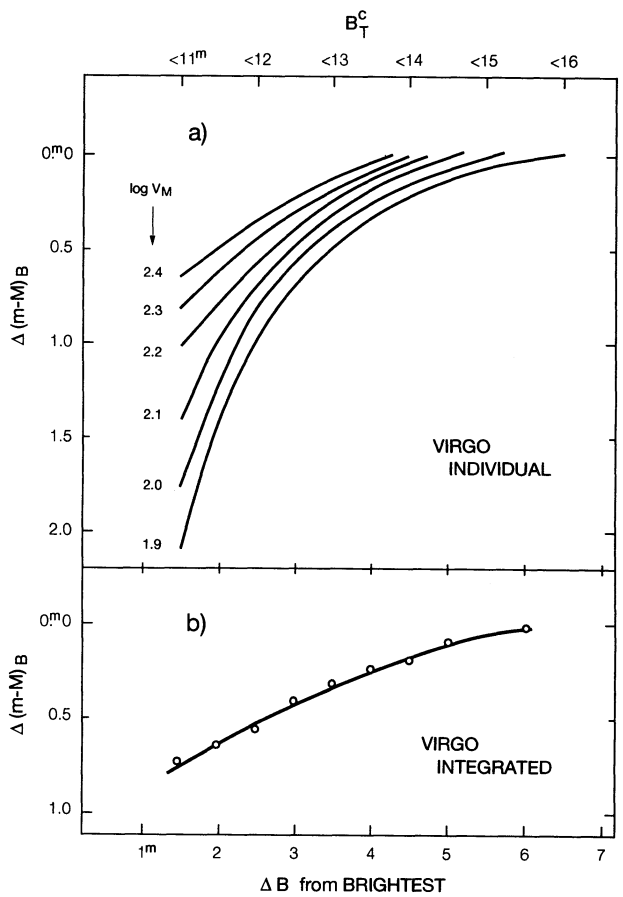

FIG. 7.—(*a*) The difference in magnitude for different rotational velocities, V_M, at the reading points of the equations in Table 2, between the equation of the regression line through the data as listed in col. (2) of Table 2 and the equation for the fiducial line drawn in each panel of Fig. 6. The difference is a function of the limiting apparent magnitude marked along the top abscissa. The ΔB values along the bottom abscissa are based on the brightest Virgo Cluster galaxy having B = 9.5 in the FBGP data. (*b*) Same as *a*, but calculated from the mean deviation of all the data points in each of the panels of Fig. 6 for all rotational velocities. This is close to the procedure that is used in practice by observers in analyzing TF data.

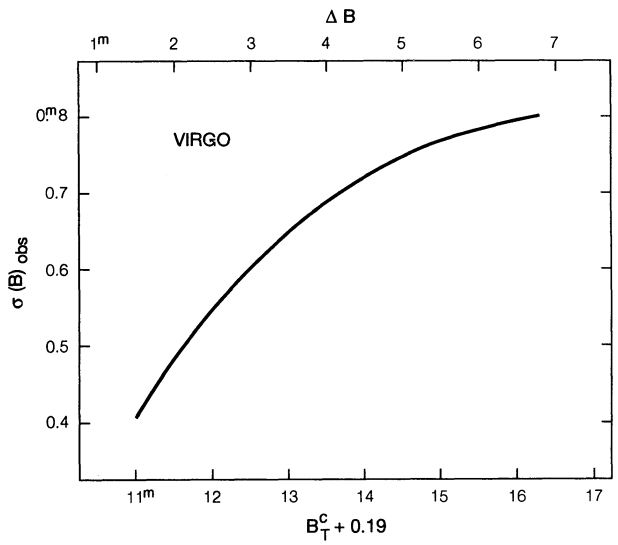

FIG. 8.—Same as Fig. 5 for the variation of the observed $\sigma(M)$ values of the TF regression with the depth of sampling into the luminosity function, but from the data in Table 2 for the Virgo Cluster in the B photometric band. Abscissa is the B_{T_c} magnitude system of FBGP but made fainter by 0.19 for zero absorption in the Galactic pole. The apparent (observed) dispersion, $\sigma(M)_{obs}$, at a given v_{rot} does not reach the intrinsic value (here taken to be 0.8 mag in B), until we have sampled ~5.5 mag into the cluster luminosity function.

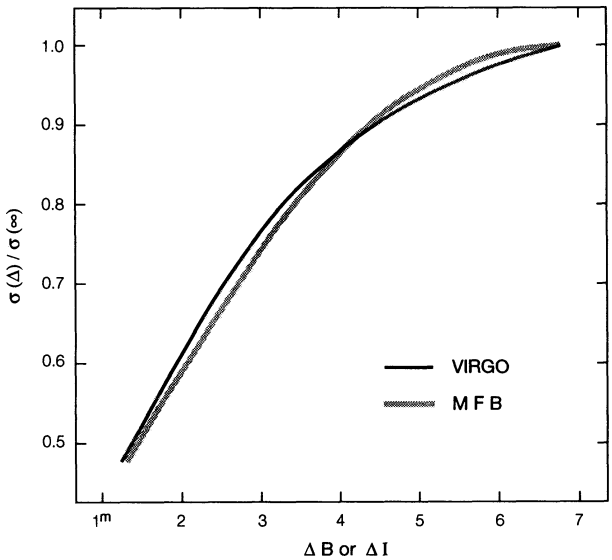

FIG. 9.—Combination of Figs. 5 and 8 but with the *percentage* (ordinate) of the intrinsic dispersion that is observed at any given magnitude grasp into the cluster luminosity function. The apparent magnitude values along the abscissa in Figs. 5 and 8 are changed into magnitude differences from the first-ranked cluster galaxies by assuming the brightest galaxy to have $B = 9.5$ in the Virgo Cluster and $I = 10.0$ mag in the MFB simulated cluster at a distance of ⟨log redshift⟩ = 3.7. The latter follows by noting the apparent magnitude of the horizontal line in Fig. 1 that is tangent to the upper envelope of the Spaenhauer configuration at log $v = 3.7$ in the upper left panel which contains the brightest galaxy.

The important result of Figure 8 is that the *intrinsic* dispersion of $\sigma(M) \sim 0.8$ mag is not reached until the cluster is sampled to a depth of ~6 mag. Part of the variation in the *apparent* $\sigma(M)$ value is a result of the progressive increase in the intrinsic dispersion as smaller rotational velocities are considered. The remaining effect is a result of the CPI bias.

Figure 8 has a larger amplitude than the similar Figure 5 for simulated clusters in the I band because the intrinsic dispersion in B is indeed slightly larger than in I [$\sigma_I(\infty) = 0.62$ mag compared with $\sigma_B(\infty) = 0.80$ mag]. The increase of the $\sigma(M)_{obs}$ values with magnitude grasp into the sample are combined in Figure 9. The ordinate is the percentage of the intrinsic dispersion for the complete sample (integrated over all line widths) reached by the observed dispersion at any given penetration into the cluster luminosity function (the abscissa).

5. THE HUBBLE CONSTANT

A purpose of this paper is to use the bias-correction machinery here and in Papers II and III to comment on the Hubble constants determined by Aaronson et al. (1986), Aaronson & Mould (1986), and Pierce & Tully (1992). All gave high values of H_0, and each neglected the CIP bias.

Each showed TF relations with very small dispersions of $\sigma(M) \sim 0.3$ mag in absolute magnitude at a given line width, which, as we have seen, are characteristic of a shallow sampling of the luminosity function. Such a small dispersion, if it were to be real, would, of course, minimize the bias effects.

That the sampling into the cluster LF is in fact this shallow, both in the clusters other than Virgo (Aaronson et al. 1986, Fig. 4), and in Virgo itself (Pierce & Tully 1988, Fig. 1), militates against claims that the intrinsic dispersion is as small as $\sigma(M) \sim 0.3$ mag.

5.1. *The Virgo Cluster Analysis*

Consider first the analysis of Pierce & Tully (1988) leading to a Virgo Cluster distance modulus[4] of $m - M = 30.96 \pm 0.20$. This distance is too small because of CPI bias.

The precise error they have made in their $(m - M)_{Virgo}$ value depends on the detailed (unknown) properties of the incompleteness of their sample. These include (*a*) whatever partial incompleteness exists in their magnitude grasp, (*b*) their incompleteness even at a given magnitude, (*c*) the distribution of v_{rot} of the sample which is required for a proper weighting of the family of curves in Figures 4 and 7, etc.

We can estimate the approximate error by adopting a factor based on Figure 1 of Pierce & Tully (1988, hereafter PT) which shows an "effective" completeness only to $\langle B_T \rangle = 12.2$. (Although their range is larger, their completeness is almost zero at $B = 13$). The number of galaxies in their Virgo sample is 29 to $B = 14$, whereas the number of galaxies used by FBGP to this limit is over 100 (but with different inclination restrictions to be sure).

Using $B = 9.5$ as the adopted magnitude of the top of the Virgo luminosity function (FBGP) gives an effective penetration into the cluster of ~2.7 mag for the PT data. Entering Figure 7*a* at a mean log V_{rot} of 2.2 (note that the PT W values are *line widths*, not rotational velocities; the two differ by ~0.3 in the log) with $\Delta B = 2.7$ mag gives an error to the modulus of ~0.5 mag caused by the bias. Therefore, taken at face value,

[4] From this modulus, these authors obtained $H_0 = 85 \pm 10$ km s^{-1} Mpc^{-1} using v(cosmic) = 1316 km s^{-1} for Virgo. Had they used the cosmic Virgo redshift reduced to the kinematic frame of the microwave background of v(cosmic) = 1179 ± 17 km s^{-1} (Jerjen & Tammann 1993) they would have obtained $H_0 = 76 \pm 8$ km s^{-1}, even with their incorrect distance modulus of 30.96.

the TF corrected modulus would be $m - M = 31.5$, $D = 20$ Mpc, and $H_0 = 59$ using the Jerjen/Tammann Machian-frame redshift of v(cosmic) = 1179 ± 17 km s^{-1} for Virgo.

However, the details of this correction are unsatisfactory at the needed level of precision. Our purpose here is only to demonstrate that the small modulus derived by PT is not itself correct as a result of the neglect of the Teerikorpi CPI bias in the presence of incomplete sampling. As stated in § 3, their appeal to front and back infall effects cannot be correct because of the close agreement between the actual Virgo data and the data for the simulated clusters in the MFB sample concerning the effects predicted in §§ 2 and 3 where infall effects are clearly absent.

The only decisive way to obtain the unbiased modulus of the Virgo Cluster using the TF method is to analyze an actual cluster sample that approaches completeness. This has been done by KKCT and by FBGP with the result that $m - M = 31.60 \pm 0.15$ using a set of calibrators (Table 1 of KKCT) that adopt modern distances to M31, M33, and M81 from, for example, Madore & Freedman (1991). With v(cosmic) = 1179 ± 17 for Virgo (Jerjen & Tammann 1993), the bias-free value of the Hubble constant adopted by KKCT is $H_0 = 56 \pm 7$ via Virgo.

The later analysis of FBGP, using an even more complete Virgo sample, gives $m - M = 31.62$, again using the modern calibrators of Madore & Freedman (1991). The resulting Hubble constant again is $H_0 \sim 56$. These various papers have been either undercited or overlooked in the literature which give encomiums for the short distance scale.

5.2. *The 10 Clusters of Aaronson et al. (1986)*

Following Bottinelli et al. (1987), we consider next the data for the 10 clusters analyzed by Aaronson et al. (1986) as discussed in the panegyric of Aaronson & Mould (1986). The data and the details of the nature of the sample are in Aaronson et al. (1986) (their Table 2 and Figure 4). They obtained $H_0 = 90$ by dismissing all biases, as they state directly.

To redress their discussion we must first reduce their distance estimates to the modern scale of the local Cepheid calibrators (Madore & Freedmann 1991). These average 0.4 mag brighter than the three calibrators (M31, M33, NGC 2403) used by Aaronson et al. (1986, their Table 3). Had they used the earlier scale of Sandage & Tammann (1974), which differs from that of Madore & Freedman by less than 0.1 mag in the mean (Tammann 1992), their zero point would have been made brighter by 0.49 mag (their estimate) and their Hubble constant reduced from 90 to 72. However, *this is still a fully biased value and is therefore still incorrect.*

An estimate of the bias correction can be made as follows. Only three of the 10 clusters have data that sample the luminosity function deeper than 4 mag (Cancer, Pegasus, and Z74-23). Of these, the authors conclude that Cancer and Z74-23 are not compact clusters but "are composed of unbound substructures strung out in space" (their Fig. 9). Of the remaining eight clusters, three (Coma, Pisces, and A1367) reach as much as 3.5 mag into the luminosity function. The remaining four (A400, A539, Hercules, and A2634/66) reach only 2 mag beyond the brightest member.

Although the material is inhomogeneous as to completeness, an estimate of an approximation correction for incompleteness can be made from Figure 7*a*. Reading the 10 panels in Figure 4 of Aaronson et al. (1986) shows that the mean log rotation velocity of the 10 clusters is near 2.3. (Recall again that LW ~ $2v_{rot}$). For the four most biased clusters where the penetration into the cluster is 2 mag (A400, A539, Hercules, A2634/66), the mean log V_{rot} is high at 2.35. Reading Figure 7*a* at this $\langle V_{rot} \rangle$ with a 2 penetration gives a bias correction of 0.55 mag for each. The $m - M$ modulus is too small by this amount.

For the three clusters with 3 mag penetration, the mean log V_{rot} is 2.28, giving a correction of 0.3 mag. For the one remaining cluster with a penetration of 4 mag (Pegasus), the mean log V_{rot} is 2.25, which requires a correction of 0.1 mag, based on Figure 7*a*.

Hence, the estimated mean correction for the eight clusters that remain in the sample, averaging 0.55 mag for four clusters, 0.3 mag for three clusters, and 0.1 mag for one cluster, is 0.40 mag. This, added to the 0.49 mag from the calibrators, gives an approximate total correction of 0.89 mag for the Aaronson et al. sample. This is a factor of 1.51 in distance, reducing their value of 90 to $H_0 \sim 60$.

Because these cluster data are too inhomogeneous as regards the incompleteness factors, we cannot claim this to be a new determination of H_0 via the TF method. Our purpose here is rather to justify the *upper envelope* fits made by KKCT to the Aaronson et al. data so as to compensate for the bias. KKCT obtained $H_0 = 57$ from the Aaronson et al. data in the following way.

Because of the faintward progression of the ridge lines of a TF diagram as the percentage of the cluster completeness increases (their Fig. 9, *which is the CPIB effect*), it is necessary to use such upper envelope fits of the TF diagrams of the 10 cluster sample of Aaronson et al. (1986). This compensates for the incompleteness factors that cause their cluster TF diagrams to differ systematically in zero point from the TF calibration that is done with *distance-limited* samples. In this way, KKCT (Fig. 9 of KKCT) derive a distance scale that gives $H_0 = 57$ with the TF method using the Aaronson et al. (1986) clusters. The analysis by KKCT also gave the distance to the Virgo Cluster as 21 Mpc (Table 6 of KKCT).

KKCT conclude that the original distance *ratios* to the 10 clusters of Aaronson et al. (1986) were nearly correct, but because of the incompleteness bias, the *absolute* distances of Aaronson et al. are too small by a factor of 1.59. This is identical, within the errors, with the factor of 1.51 found independently here.

We would finally note that Bottinelli et al. (1986, 1987) discussed the CPI bias, showing that allowing for it leads to $H_0 = 56$ instead of $H_0 = 90$ when the local distance scale set up by Sandage & Tammann (1974, hereafter ST) is used. These ST values for the distance modulii of the local calibrators average 0.55 mag larger than those used by de Vaucouleurs (1979a) for the same local galaxies (Table 5 of Bottinelli et al. 1986).

5.3. *H_0 from TF Field Galaxies*

The TF method applied to *field galaxies* in a distance-limited sample has always required the long distance scale. For example, the distance-limited 500 km s^{-1} catalog of Kraan-Korteweg & Tammann (1979) gives H_0 between 48 and 56 using the 21 cm line width data of Huchtmeier & Richter (1986), and calibrated with the 64 galaxy sample of Richter & Huchtmeier (1984). The difference between this distance-limited sample and the fully biased field galaxy sample of Aaronson et al. (1982) was emphasized again as resulting from selection bias in Sandage (1988, Fig. 9; 1994b).

These field-galaxy demonstrations have been criticized in the literature, we believe incorrectly, on the basis that the *cluster* data consistently give $H_0 \sim 90$, and therefore the field galaxy samples have been claimed to be incorrect based on the false precept that "cluster data, where all galaxies are at the same distance, cannot be biased."

Also, as mentioned earlier, another criticism of the field galaxy data has been that the local velocity field is so badly fouled by noncosmological streaming and random motions that kinematic distances are more incorrect than photometric distances. The consequence is said to be that an "*incorrectly large* intrinsic dispersion of the TF relation is derived" (a summary of the Aaronson et al. and Pierce & Tully position). A purpose of this paper (Figs. 8–9) is to belie this precept.

That such noncosmological kinematic effects do not occur at a level that fouls the analysis has been shown elsewhere (Sandage & Tammann 1975, 1990; Sandage 1972, 1994a, b, 1995; Federspiel et al. 1994; Tammann & Sandage 1995a, b) based on the nature of the residuals in Hubble diagrams.

Finally, proof that the distance scale set out by de Vaucouleurs (1979b), based on his several criteria, and by Pierce (1994), based on the TF method, are incorrect is seen by the mean absolute magnitude of SNe Ia at maximum calibrated via Cepheid distances to parent galaxies. De Vaucouleurs (1979b, his Table 9) requires $\langle M_B(\max)\rangle = -18.5 \pm 0.2$ for SNe Ia on his distance scale. Pierce (1994, his Table 2), basing his scale solely on the TF method, requires $\langle M_B(\max)\rangle = -18.74 \pm 0.14$. Both calibrations are ~ 1 mag fainter than $\langle M_B(\max)\rangle = -19.65 \pm 0.13$ calibrated by Saha et al. (1995), based on Cepheids. Pierce's claim that if $H_0 \sim 45$, then the TF relation "must then have a discontinuous absolute magnitude calibration of $\Delta m = 1.4$ mag over a small range in distance, namely $4.0 < D_{TF} < 6.5$ Mpc" is incorrect. It arises from the neglect of the bias corrections that *vary with distance* (Fig. 8 of Federspiel et al. 1994), and can therefore imitate a step, as is also apparent in de Vaucouleurs & Peters (1986), where the same effect occurs as an artifact of the uncorrected bias.

Hence, the conclusion that follows both here and from Papers II and III of this series is that the bias problem in the Tully-Fisher method is complicated, and that its effects are remarkably severe, making clear that values of $H_0 \sim 90$ based on biased TF relations need substantial corrections downward.

The principal problem now concerning H_0 is not the distances to the local calibrators (we counter Aaronson 1987) but rather rests with the *bias problems*. The severity of the bias depends on the intrinsic dispersion of the TF relation. Decisive means must be devised to determine this intrinsic dispersion precisely, otherwise the debate on the value of H_0 will continue.

The science and the first drafts of this paper were made at the Institute of Astronomy of the University of Basel in 1994 May/June. A. S. is grateful for the hospitality of the Institute during this extended visit, where the many contacts with the staff were invaluable. We also thank the Swiss National Science Foundation for its support of the Institute, and thank also the US National Aeronautics and Space Administration (NASA) for a grant through the Space Telescope Science Institute for the determination of the Hubble constant using the *Hubble Space Telescope*. We are grateful to a perceptive referee who advised us well on the first draft of this paper. We are also grateful to Donald Lynden-Bell for his comments on the inverse relation and its bias properties.

APPENDIX

A literature has grown concerning the advantage of using the inverse regression of $\log v_{rot}$ on M rather than M on v_{rot} for the TF formulation. Schechter (1980) suggested that the former avoids the bias in the slope.

A particularly powerful demonstration of the Schechter "inverse" prediction that the slope remains constant was made by FBGP (their Fig. 7), using Virgo Cluster data that penetrate 6 mag into the luminosity function.

However, the impression is incorrect that because the inverse *slope* is constant, that then the inverse TF formulation avoids the bias. There will be bias both in the derived (albeit constant) slope and also in the zero point if the sample is not complete in LW at a given M. This was demonstrated by Teerikorpi (1990) with an elegant formalism and was shown using actual data by FBGP. These latter authors analyze the problem in both ways (direct and inverse) and show directly from the data that bias does exist as a function of depth of penetration into the luminosity functions in both formulations. The problem is also discussed by Bottinelli et al. (1986) and by Lynden-Bell et al. (1988) as to why the direct formulation, used with its explicit correction for bias, is preferred. We are content here to illustrate the problem using the MFB data by constructing diagrams similar to Figures 2 and 3, but using the *inverse* TF regression with absolute magnitude as the independent variable.

We demonstrate Teerikorpi's (1990) conclusion that the inverse is not generally bias free if there are restrictive cuts of any kind by line width. Such restrictive cuts (natural or forced) in line width are the usual case for various obvious and unobvious reasons.

For the demonstration, we use the data for the simulated cluster from the MFB data in the highest redshift interval ($3.6 < \log$ redshift < 3.8). The subset of the data in this redshift interval is cut at progressively tighter rotational velocity limits, *but retaining all apparent magnitudes*. This is the parallel experiment as in Figures 2 and 3, but made now by cutting the other (LW) coordinate rather than absolute magnitude, dictated by an apparent magnitude limit.

The equivalent of Figure 3 (note the same redshift interval in both diagrams) is shown in Figure 10 as a series of TF diagrams such that data for *all I* magnitudes in the MFB sample in this redshift range are plotted with $\log v_{rot}$ values, but cut at $\log v_{rot}$ limits of >2.4, >2.3, >2.2, etc. The fiducial line drawn in each of the panels is the unbiased TF relation (inverse) calculated from the distance-limited subset of the total MFB sample that was isolated in Paper III (Fig. 7 there) and discussed in § 3 here. Its equation is $M_I = -9.01 \log v_{rot} - 1.95$.

The progressive deviation of the data points from the fiducial line, as the rotational velocity limits are tightened, is evident. This either is, or is related to, the inverse cluster population incompleteness bias first discussed by Teerikorpi (1990).

An additional problem with using the inverse TF relation is that it uses the absolute magnitude M as the independent variable, which is unknown a priori. In the case of clusters, one can of course use the apparent magnitude instead, but only if all sample

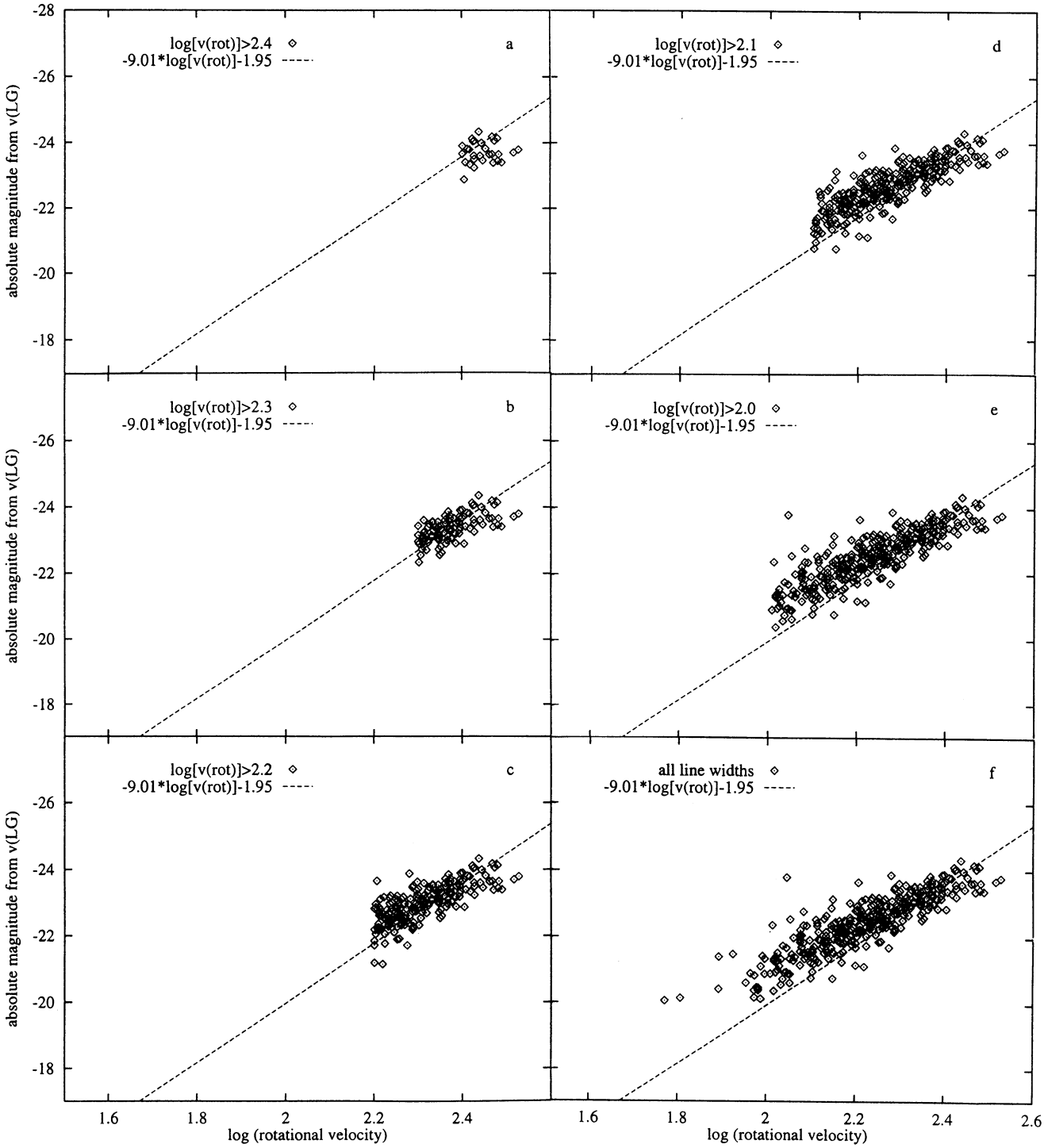

FIG. 10.—Demonstration of the bias, similar to that in Figs. 2–3, but now cutting the sample in the simulated MFB cluster at $\langle \log v \rangle = 3.7$, in intervals of rotational velocity (all apparent magnitudes included) rather than in apparent magnitude (all rotational velocities included). The fiducial line drawn in each panel is the unbiased "inverse" regression calculated from the distance-limited MFB subsample isolated in Paper III (Fig. 7 there). The equation of this line is $M_I = -9.01 \log v_{\rm rot} - 1.95$, which is the least-squares solution of the unbiased sample calculated in the inverse way (with LW as the independent variable). The deviation of the data points from this fiducial line *is* the effect of the incompleteness bias.

galaxies are cluster members. In real applications the method is therefore blind in separating true and projected cluster members, and even more so in discovering any true three-dimensional structure of a cluster. The problem is especially serious because one believes that the spirals (the only morphological types to which the TF method can apply) do not define the same spatial arrangement as the ellipitical galaxies that generally define the core of a cluster.

The corresponding problem for noncluster ("field") galaxies is that one must assume an ideal expansion field to obtain a measure of the "independent" (if one wishes to use the inverse method) variable M. One then automatically denies any peculiar or streaming motions. Hence, there is a built-in contradiction in the inverse method when the TF indicator is used to derive putative deviations from the Hubble flow.

In the current literature one, of course, attempts to recover any peculiar motions by iteration, but this procedure always rests on the assumption of minimum scatter, which we are contesting here, claiming that most, if not all, of the scatter in the TF relation is a result of *absolute magnitude* variations (a broad luminosity function) rather than peculiar motions.

One of the purposes of this paper is to prove this contention that the intrinsic dispersion of the TF method is large near $\sigma(M) = 0.7$ mag in B by using "local" field galaxies where the velocity field is known to be very quiet (§ 3). The same demonstration was made earlier (Sandage 1988) using the 500 km s^{-1} sample of Kraan-Korteweg & Tammann (1979).

REFERENCES

Aaronson, M. 1987, in IAU Symp. 124, Observational Cosmology, ed. A. Hewitt, G. Burbidge, & L. Z. Fang (Dordrecht: Reidel), 197
Aaronson, M., Bothun, J., Mould, J., Huchra, J., Schommer, R. A., & Cornell, M. E. 1986, ApJ, 302, 536
Aaronson, M., et al. 1982, ApJS, 50, 241
Aaronson, M., & Mould, J. 1986, ApJ, 303, 1
Aaronson, M., Mould, J., Huchra, J., Sullivan, W. T., III, Schommer, R. A., & Bothun, G. D. 1980, ApJ, 239, 12
Bernstein, G. M., Guhathakurta, P., Raychaudhury, S., Giovanelli, R., Haynes, M. P., Herter, T., & Vogt, N. P. 1994, AJ, 107, 1962
Bottinelli, L., Fouqué, P., Gouguenheim, L., Paturel, G., & Teerikorpi, P. 1987, A&A, 181, 1
Bottinelli, L., Gouguenheim, L., Paturel, G., & Teerikorpi, P. 1986, A&A, 156, 157
Burstein, D., & Raychaudhury, S. 1989, ApJ, 343, 18
de Vaucouleurs, G. 1979a, ApJ, 227, 380
———. 1979b, ApJ, 227, 729
de Vaucouleurs, G., & Peters, W. L. 1986, ApJ, 303, 19
Federspiel, M., Sandage, A., & Tammann, G. A. 1994, ApJ, 430, 29 (Paper III)
Fouqué, P., Bottinelli, L., Gouguenheim, L., & Paturel, G. 1990, ApJ, 349, 1 (FBGP)
Huchtmeier, W. K., & Richter, O.-G. 1986, A&AS, 63, 325
Jacoby, G. H., et al. 1992, PASP, 104, 599
Jerjen, H., & Tammann, G. A. 1993, A&A, 273, 354
Kraan-Korteweg, R. C., Cameron, L. M., & Tammann, G. A. 1988, ApJ, 331, 620 (KKCT)
Kraan-Korteweg, R. C., & Tammann, G. A. 1979, Astron. Nachr., 300, 181
Lynden-Bell, D., Faber, S. M., Burstein, D., Davies, R. L., Dressler, A., Terlevich, R. J., & Wegner, G. 1988, ApJ, 326, 19
Madore, B. F., & Freedmann, W. L. 1991, PASP, 103, 933
Mathewson, D. S., Ford, V. L., & Buchhorn, M. 1992, ApJS, 81, 413
Pierce, M. 1992, in Jacoby, G. H., et al. 1992, PASP, 104, 599
———. 1994, ApJ, 430, 53
Pierce, M., & Tully, R. B. 1988, ApJ, 330, 579
———. 1992, ApJ, 387, 47
Richter, O.-G., & Huchtmeier, W. K. 1984, A&A, 132, 253
Saha, A., Sandage, A., Labhardt, L., Schwengeler, H., Tammann, G. A., Panagia, N., & Macchetto, F. D. 1995, ApJ, 438, 8
Sandage, A. 1972, ApJ, 178, 1
———. 1975, ApJ, 202, 563
———. 1988, ApJ, 331, 605
———. 1994a, ApJ, 430, 1 (Paper I)
———. 1994b, ApJ, 430, 13 (Paper II)
———. 1995, in The Deep Universe, ed. B. Binggeli & R. Buser (Berlin: Springer), pp. 91–126, 211–233
Sandage, A., & Tammann, G. A. 1974, ApJ, 190, 525 (ST)
———. 1975, ApJ, 197, 265
———. 1990, ApJ, 365, 1
Schechter, P. L. 1980, AJ, 85, 801
Tammann, G. A. 1992, Phys. Scr., T43, 31
Tammann, G. A., & Sandage, A. 1995a, in IAU Symp. 168, in press
———. 1995b, in Current Topics in Astrofundamental Physics, ed. R. Sanchez, in press
Teerikorpi, P. 1987, A&A, 173, 39
———. 1990, A&A, 234, 1
Willick, J. 1994, ApJS, 92, 1